Polymer 54 (2013) 5050–5057

Contents lists available at SciVerse ScienceDirect

Polymer

journal homepage: www.elsevier.com/locate/polymer

Tautomerizable styrenic copolymers confined in AAO templates

Juan M. Giussi [a,b,c], Iwona Blaszczyk-Lezak [a], Patricia E. Allegretti [b], M. Susana Cortizo [b,c], Carmen Mijangos [a,*]

[a] Instituto de Ciencia y Tecnología de Polímeros, CSIC, Juan de la Cierva 3, 28006 Madrid, Spain
[b] Laboratorio de Estudio de Compuestos Orgánicos (LADECOR), Facultad de Ciencias Exactas, UNLP (1900), 47 y 115, La Plata, Argentina
[c] Instituto de Investigaciones Fisicoquímicas Teóricas y Aplicadas (INIFTA), CCT-La Plata, Facultad de Ciencias Exactas, UNLP (1900), Dg 113 y 64, La Plata, Argentina

ARTICLE INFO

Article history:
Received 11 October 2012
Received in revised form
10 June 2013
Accepted 17 June 2013
Available online 3 July 2013

Keywords:
Tautomeric copolymers
AAO templates
Nanostructured scaffolds

ABSTRACT

The aim of this work is to prepare new keto-enol tautomerizable polystyrene copolymer nanofibers, by infiltrating the polymer into nanoporous anodized aluminum oxide (AAO) nanocavities, and to examine the influence of confinement effects on the polymer properties of nanostructured polymers in comparison to the bulk. The interest of this work lies, on the one side, on the presence of tautomeric groups that could lead to discriminate against specific substrates and, therefore, could make them interesting in biomedicine. And, on the other hand, on the topographic characteristic of oriented nanofibrous structures that could be convenient for cell regeneration.

In this work nanostructured keto-enol tautomerizable polystyrene copolymer nanofibers, i.e. Styrene-co-2-methyl-3-oxo-5-phenyl-4-pentenonitrile (St-co-MOP) of different chemical composition, have been prepared under soft infiltration conditions of the polymer into AAO templates. For all compositions, SEM images show stacked nanofibers reproducing the dimensions of AAO nanopores and Raman confocal spectroscopy of the samples, confirms the homogenous chemical distribution of nanofibers through all the length of AAO pores. The glass transition temperature values for St-co-MOP copolymer nanofibers inside AAO nanocavities determined by differential scanning calorimetry are higher than those corresponding to the bulk copolymers. From thermograms of nanofibers obtained by thermo gravimetric analysis (TGA), in an air atmosphere, the existence of two thermal peaks is observed, the second one probably caused by the presence of tautomeric forms in the copolymers. Moreover, the elastics moduli found for the bulk copolymers are consistent with their employment for building extracellular matrices.

In summary, this study clearly demonstrates the feasibility of producing nanofibers from styrene-co-2-methyl-3-oxo-5-phenyl-4-pentenonitrile (St-co-MOP) tautomeric polymers with a high degree of homogeneity and appropriate thermal and mechanical properties. Furthermore, preliminary results for tautomeric copolymers do not show cytotoxic effects, indicating that the obtained nanostructured copolymer combines several relevant properties required for its future applications as a biomaterial for cell scaffolds.

1. Introduction

Simple fabrication of one-dimensional polymer and polymer based composite nanostructures by the so called “template method”, i.e. polymer infiltration inside the nanonoporous of anodized alumina template (AAO), has attracted increasing interest due to the possibility of obtaining polymers with different morphologies, i.e. nanofibers, nanorods, nanotubes or coaxial nanofilm from almost any kind of homopolymer [1–13]. It has also been reported that a polymer confined into nanocavities exhibits different properties from those of the bulk, i.e. differences in the early stages of the crystallization [14,15], in the glass transition values, chain dynamics [16,17], and so on. Moreover, according to the literature, 1D nanostructures are of exceptional interest due to their potential applications in biomedicine, photonics, magnetic labeling, etc [10,18–22]. In particular, as reported by other teams and from our own investigations, these materials have attracted considerable attention due to their biocompatibility and high accessible surface area which greatly enhance the stability and the amount of immobilized enzymes and cells [23–25]. Moreover,

* Corresponding author.
E-mail address: cmijangos@ictp.csic.es (C. Mijangos).

0032-3861/$ – see front matter © 2013 Elsevier Ltd. All rights reserved.
http://dx.doi.org/10.1016/j.polymer.2013.06.040

some authors found that scaffolds with ordered surface morphology improve the cellular biocompatibility. For instance, Cortizo et al., demonstrated that adhesion, proliferation and mineralization were significantly improved when cells were grown on parallel-arranged collagen fibers [26] and Wang et al. suggested that osteoblast-like cells prefer randomly-oriented PLLA nanofibrous scaffolds [27]. Therefore, the topographic characteristic of oriented nanofibrous structures should be convenient for bone tissue regeneration.

Synthetic polymers containing tautomeric functional groups have emerged as important materials due to their potential applications [28,29]. The interest in this type of polymers lays on the possibility of regulating the composition of both tautomeric forms (keto-enol) to obtain polymeric materials with changeable polarity as a function of the surrounding environment. In connection to their potential applications, subject of future work, numerous cellular processes have been reported to occur through tautomeric forms of certain compounds. For instance, Benner discussed different ways in which organic chemistry can be the producer of artificial DNA molecules that have broad therapeutic applications in diagnostic tests for disease treatment [30]. Especially important is the presence of tautomeric groups in these molecules for that they are discriminated against specific substrates according to the environment in which they exist and, therefore, could make them interesting in biomedicine.

Clearly a polymeric material that presents the two aforementioned structural features, biz. tautomeric functional groups and the feasibility to transform into a nanostructured matrix, would be a very promising biomaterial. In this sense, the first step, i.e. the polymerization of a new kind of keto-enol tautomerizable copolymers, i.e. styrene-co-2-methyl-3-oxo-5-phenyl-4-pentenonitrile (St-co-MOP) copolymers and their chemical and physical characterization, has recently been carried out and reported elsewhere [31]. The second step, the production of nanofibers from these copolymers is the subject of the present work.

The aim of the present work is to report, for the first time, the fabrication of tautomerizable copolymer nanofibers, composed of styrene (St) and 2-methyl-3-oxo-5-phenyl-4-pentenonitrile (MOP), by infiltration of the melt copolymer in the nanocavities of laboratory made hard alumina templates and to study the main properties of the copolymer nanofibers. It includes the comparison between the properties of these copolymers in bulk and nanostructured. To achieve the above objectives, porous anodic aluminum oxide (AAO) templates have been obtained by a two anodization process.

2. Experimental

2.1. Copolymer synthesis and characterization

Tautomerizable styrene-co-2-methyl-3-oxo-5-phenyl-4-pentenonitrile copolymers (St-co-MOP), of different MOP monomer mole fraction in the copolymer (F_{MOP}), were synthesized by Giussi et al. as described elsewhere [31]. In this work, three of these copolymers, St-co-MOP_1, St-co-MOP_2 and St-co-MOP_3 were used for preparing polymer nanostructures. The chemical composition and weight-average molecular weight (M_w) are: St-co-MOP_1, $F_{MOP} = 0.17$ and $M_w = 82{,}000$ g/mol; St-co-MOP_2, $F_{MOP} = 0.38$ and $M_w = 64{,}000$ g/mol and St-co-MOP_3, $F_{MOP} = 0.62$ and $M_w = 37{,}000$ g/mol. Monomers and copolymers have been characterized by nuclear magnetic resonance (NMR) and Infrared (IR) spectroscopies. These techniques have allowed assessing the tautomeric equilibrium existing both in the monomer and the copolymers [31]. Scheme 1 shows the structure of tautomeric equilibrium on the copolymer synthesized. Polystyrene (PS) (Melt Index 7.5 Aldrich, $M_w = 192{,}000$ g/mol) was also used as a standard for comparison.

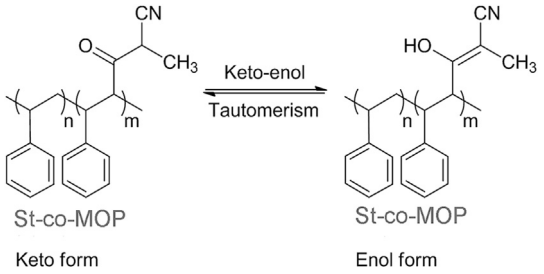

Scheme 1. Structure of Styrene-co-2-methyl-3-oxo-5-phenyl-4-pentenonitrile copolymer (St-co-MOP) through of keto-enol tautomers.

2.2. AAO templates

Two types of anodized aluminium oxide templates (AAO) have been prepared via a two-step electrochemical anodization process on Aluminium sheets (99.999% degree) of around 10 cm^2, as described elsewhere [2,32–34]. Subsequently, a first anodization is performed in an acidic electrolyte, oxalic or sulfuric acid, under constant voltage; then, the first alumina layer is dissolved and finally the second anodization is carried out. The obtained AAO templates were annealed at 200 °C in vacuum in order to remove the possible adsorbed organic molecules from the pore walls. As it will be shown after, the diameters of nanocavities are 35 and 28 nm. For a detailed description of the process see for instance Ref. [1].

2.3. Infiltration of copolymer

The infiltration of St-co-MOP copolymers and commercial PS into the AAO nanocavities was carried out via the melt precursor film wetting method, as described by Martín et al. [2]. For that, solid copolymer was placed on the AAO surfaces and then infiltrated at the corresponding temperatures and time (see Table 1 for details). During this process, the polymer was pressed over the template every 15 min to promote infiltration. Three copolymers, St-co-MOP_1, St-co-MOP_2 and St-co-MOP_3 and PS were infiltrated into AAO template of an average diameter of 35 nm. For comparison St-co-MOP_2 was also infiltrated into AAO template of around 28 nm diameter. As represented in Scheme 2, the solid copolymers were placed on the AAO surfaces and introduced in an oven, at a temperature about 100 °C higher than the copolymer glass transition temperature (T_g), under nitrogen atmosphere and the time of infiltration was varied depending on copolymer composition (1). After the infiltration process, the excess of copolymer was removed from the surface of AAO template (2).

2.4. Chemical and morphological characterization

In order to characterize the polymer nanostructures by different techniques, the samples were submitted to different treatments, depending on the method used. The steps for sample preparation are illustrated in Scheme S1 of Supporting Information.

Table 1
Copolymer composition and experimental conditions of the infiltration process of St-co-MOP copolymers and PS with corresponding infiltrated weight.

Polymer template	Polymer composition (F)	T (°C)	Time of infiltration (minutes)	Infiltrated weight (mg)
n-PS	–	210	300	11.2 ± 0.1
n-St-co-MOP_1	0.17	217.5	225	13.3 ± 0.1
n-St-co-MOP_2	0.38	220	300	13.5 ± 0.1
n-St-co-MOP_3	0.62	230	360	12.3 ± 0.1
n_{28}-St-co-MOP_2	0.38	220	360	11.7 ± 0.1

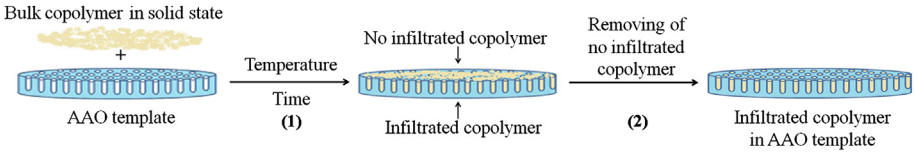

Scheme 2. Graphical representation of infiltration procedure.

2.4.1. Scanning electron microscopy

The AAO templates and all the infiltrated samples were morphologically characterized by scanning electron microscopy (SEM) (Philips XL-30 ESEM). In order to perform the analysis of free copolymer nanofibers, the aluminum substrate was treated with a mixture of HCl, $CuCl_2$, and H_2O and the alumina was dissolved in 5% wt H_3PO_4. Previously, in order to support the free nanostructures, a coating was placed over the template; see for details Scheme S1 of Supporting Information.

2.4.2. Raman spectroscopy

The obtained copolymer nanofibers were characterized by Raman Spectroscopy, Renishaw InVia Raman Microscope. The measurements have been carried out with the filled template, that is, the aluminum, alumina and copolymer inside the nanocavities (see Scheme S1 of Supporting Information). The Raman scattering was excited with a 785-nm near-infrared diode laser. A 100×, NA090 objective lens was used, giving a laser spot diameter of ~1 μm. With this objective the sampling depth is estimated to be around 4–5 μm (half-width of the confocal depth profile for a silicon wafer) and the lateral resolution is estimated at about 1 μm with the system operated in the confocal mode. Raman scattered radiation was focused through a pinhole aperture. The methodology has been described by Maiz et al. [12]. Data acquisition covered the spectral range 3600–100 cm^{-1} with a spectral resolution of 4 cm^{-1} for each exposure of the CCD detector. Depth profiles were obtained by focusing the microscope stepwise, at 10 μm intervals through the AAO template.

2.5. Thermal properties of nanostructured copolymer

2.5.1. Glass transition temperature

In order to determine the glass transition temperature value of copolymers by Differential Scanning Calorimetry (DSC), analysis has been carried out directly on infiltrated polymers into alumina pores, without aluminium (see Scheme S1 of Supporting Information). The aluminum was removed following a previous treatment with an aqueous solution of $CuCl_2$ and HCl, as was reported elsewhere [12]. All the experiments were carried out on a DSC 8500 Hyper DSC-Perkin Elmer, in nitrogen atmosphere, at 20 °C/min of heating and cooling rate, from room temperature to 230 °C.

2.5.2. Thermal stability

The thermal stability of copolymers in AAO nanocavities was determined by thermo gravimetric analysis in TGA Q500-TA Instruments equipment, under nitrogen and air atmosphere, from room temperature up to 900 °C and gas purged at 90 ml/min. As in Raman spectroscopy analysis, the study through this methodology has been carried out without any previous treatment, for an aliquot of complete template (see Scheme S1 of Supporting Information).

2.6. Mechanical properties

Mechanical properties of the copolymers and PS were measured with an Instron instrument (Instron3366, INSTRON Co., Ltd.) by using a dumbbell shaped specimen of 50 mm length with a neck size of 10 mm length 5 mm width. The specimens were tested with a grip distance of 22 mm and a crosshead speed of 10 mm/min at room temperature by using a standard method. Ultimate tensile stress, elastic moduli, as well as elongation-at-break were calculated on the basis of the generated tensile stress–strain curves. Three specimens were analyzed for each sample, then their values were averaged and the results are expressed as the mean ± SEM.

3. Results and discussions

3.1. Fabrication of AAO templates

The synthesis of AAO templates has been described in the experimental section and the morphological characterization carried out by scanning electronic microscopy. The study through this technique allows to examine both the surface and length of the AAO templates. Fig. 1 shows SEM micrographs of synthesized AAO templates at different magnifications: a and b corresponding to AAO templates obtained in sulfuric acid. It is observed that the dimensions of the pore nanocavities are very homogeneous and around 28 nm of diameter; c and d correspond to AAO templates obtained in oxalic acid. It is also observed that the dimensions of the pore nanocavities are very homogeneous and around 35 nm of diameter and e and f show the perpendicular view for the last template. From Fig. 1e is observed that the length of the nanocavities is 80 μm. Although not shown here, the length of the pores in the first templates is also 80 μm. From these figures we can conclude that the nanoporosity of templates is highly regular in size and order; in other words, the same diameter is maintained all along the length of the pores. In Fig. 1f, the nanocavities are observed in more detail.

3.2. Infiltration of copolymers

As reported in the experimental section, three bulk St-co-MOP copolymers of different compositions have been synthesized and analyzed. The molar composition of the copolymers (F_{MOP}), vary from 0.17 to 0.62. These three bulk copolymers and PS were infiltrated into AAO templates with an average diameter of 35 nm. Bulk copolymers and polystyrene, hereafter, be referred to as *b*-St-co-MOP_x and *b*-PS and infiltrated St-co-MOP copolymers and PS into 35 nm AAO template referenced as *n*-St-co-MOP_x and *n*-PS, respectively. The subscript *x* designates the copolymers of different compositions, while *b* and *n* indicate "bulk" and "nanostructured", respectively. Copolymer St-co-MOP_2 was also infiltrated into AAO template of 28 nm of diameter and referenced as n_{28}-St-co-MOP_2. In Table 1 the sample compositions and the experimental conditions of the infiltration process are listed, that is, the temperature and time of infiltration. Moreover, the same table collects the final weight (in mg) of infiltrated copolymers into the nanocavity. It is important to mention that these values correspond to almost completely filling nanocavities, as it will be confirmed later.

The wide range of F_{MOP} will allow us, in principle, to obtain a greater or smaller variation in the spectrum of properties of the polymers as a function of the composition and to establish the

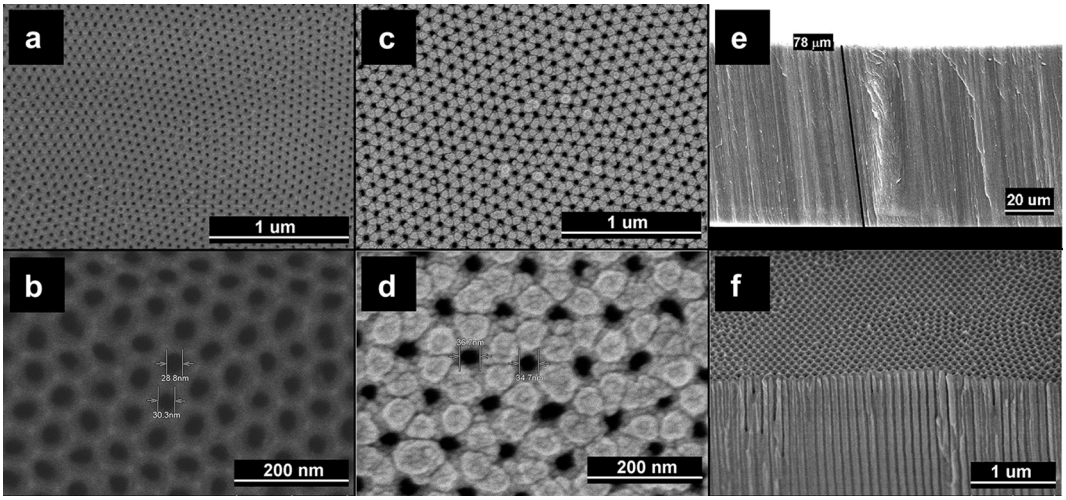

Fig. 1. SEM micrographs of surfaces of prepared AAO templates at different magnifications: (a) and (b) 28 nm top view, (c) and (d) 35 nm top view, (e) and (f) 35 nm side view.

differences, if any, between the bulk and nanostructured copolymer. Moreover, as recently reported, the tautomeric equilibrium shows a dependency with monomer molar fraction of the copolymers (F_{MOP}) and with the nature of solvent: when F_{MOP} increases, the enol fraction (x_{enol}) in $CHCl_3$ increases, while (x_{enol}) decreases in CH_3CN. Also was observed that at same F_{MOP} values, x_{enol} increase when the solvent polarity increasing, suggesting the existence of different types of interactions between keto-enol tautomeric forms according to the copolymer composition and solvent polarity. Therefore, the variation in the monomer molar fraction in the copolymer (F_{MOP}) could allow an evaluation, if any, of the effect of this variable in the nanostructuration and properties of the copolymers.

As a first approach, it is observed that as F_{MOP} value increases, the temperature and time of infiltration process increases, being in agreement with the lower chain mobility of the copolymer, as it will be reported later on, by DSC analysis. It is important to mention that, the infiltration process of this kind of copolymers is much faster (less than 6 h) and it is also a lower energetic process in comparison to block copolymers and many other polymers recently studied.

3.3. Morphological characterization

The morphological study through scanning electronic microscopy technique allows examining the copolymer nanofibers out of AAO template. Fig. 2 shows the nanofibers obtained by infiltration into AAO template (a–f) at different magnifications, Fig. 2a and b; Fig. 2c and d and Fig. 2e and f correspond to micrographs of the extracted St-co-MOP_1, St-co-MOP_2 and St-co-MOP_3 copolymers nanofibers from AAO of 35 nm of diameter, respectively. Fig. 2g and h show micrographs of the St-co-MOP_2 nanofibers extracted from an AAO template of 28 nm of diameter at two different magnifications.

From Fig. 2 it can be deduced, in the first place that the nanofibers of the three copolymers exhibited regular shape and second, nanofibers reproduce the diameter of AAO template along a sufficient length. Therefore, the micrographs confirm the appropriate filling of the nanocavities. These results allow us to conclude the precise adjustment of fiber aspect ratio and the high production of nanofibers/cm^2 of template, 10^9, obtained by the easy polymer infiltration process into AAO nanocavities.

At greater magnification of micrographs (Fig. 2b, d, f and h), it is not possible to observe a single nanofiber but associated ones, of at least two of them, so it seems evident that some kind of interaction between nanofibers exists. This kind of interactions could results of hydrogen bond interaction due to the highest content of the enol tautomer in the polar environment of AAO template. Similar results were found in our previous study of a MOP copolymer in solution in which we demonstrated that the enol polymer fraction increase when the solvent polarity increases, due to the favored hydrogen bond intrachain. Fig. 2g shows a perfect regularity and homogeneity for n_{28}-St-co-MOP_2 nanostructures. In this case, it is also observed that n_{28}-St-co-MOP_2 nanofibers are interacting with each other, which is consistent with its smaller diameter. These increased interactions could explain the obtained higher order. This behavior indicates that the diameter of template is crucial in the acquired order of the nanofibers.

3.4. Chemical characterization

Raman spectroscopy is employed for the first time in the literature to chemically characterize and determine the homogeneous distribution of copolymer nanofibers within AAO templates. A previous study has been performed with bulk copolymers. Fig. 3a shows Raman spectra for the three *b*-St-co-MOP copolymers and *b*-PS in which the main bands of the polymers are easily observed and identified. As observed, the spectra of copolymers show new signals in comparison to *b*-PS due the presence of MOP monomer in the copolymer. According to the literature, the signal at 2230 cm^{-1}, has been assigned to the nitrile group in the copolymers [35]. The intensity of this band increases from the *b*-St-co-MOP_1 to *b*-St-co-MOP_3, in agreement to the increase of the MOP monomer molar fraction in the copolymer.

In order to analyze the copolymer distribution along the pore nanocavities, a calibration has been performed with the bulk copolymers. Although not shown here, the calibration curve is obtained from the relation I_{CN}/I_{Ar} versus composition, F_{MOP}. I_{CN} being the intensity of signal at $\sim$2200 cm^{-1}, corresponding to nitrile stretching frequency and, therefore, only presented in the MOP monomer and, I_{Ar}, being the intensity of signal at $\sim$1000 cm^{-1} corresponding to out of plane CH aromatic deformation vibration, presented in both monomers, St and MOP, therefore, it represents 100%. The measurements have been made at different points of the sample and statistical analysis has been performed. For *b*-St-co-MOP_1 copolymer, the relation $I_{CN}/I_{Ar} = 0.34 \pm 0.03$.

Unlike the morphological study using SEM, Raman spectroscopy method has enabled to evaluate the presence of copolymers along the length of nanocavity, through the confocal methodology. While all three copolymers have been studied by Raman confocal

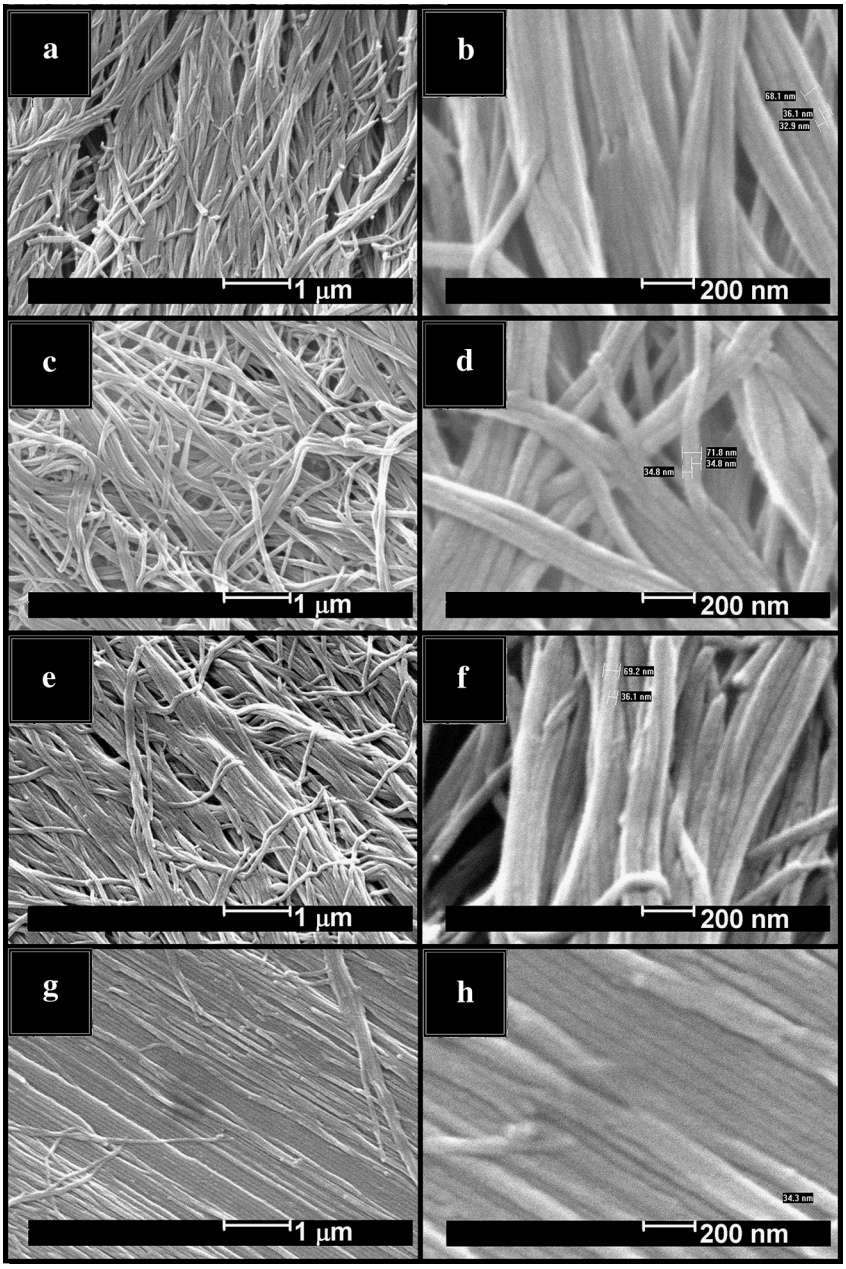

Fig. 2. SEM micrographs of free nanofibers at different magnifications: (a) and (b) *n*-St-co-MOP$_1$, (c) and (d) *n*-St-co-MOP$_2$, (e) and (f) *n*-St-co-MOP$_3$, and (g) and (h) n_{28}-St-co-MOP$_2$.

spectroscopy, the spectrum of *n*-St-co-MOP$_1$ shows the best resolution of bands, since softer conditions of the infiltration process have been used by comparison with those for *n*-St-co-MOP$_2$ and *n*-St-co-MOP$_3$ (see Table 1). During this process, in the case of St-co-MOP$_1$, the temperature was lower than 220 °C and the exposure time was the least. As previously reported, the effect of high temperature affects the fluorescence of the AAO template and this phenomenon alter the Raman spectra as indicated by Blaszczyk-Lezak et al. and Du et al. [36,37].

Fig. 3b shows the Raman spectra of *n*-St-co-MOP$_1$ with pinhole, taken at different intervals. Despite the noise due to the fluorescence of the alumina, it is possible to observe all the characteristic bands of St-co-MOP$_1$ in the spectra, up to 60 μm. As it has been reported [38], the decrease in the intensity of the bands with the depth of the cavity is due to the less transparency of the sample with the profundity.

From the *n*-St-co-MOP$_1$ copolymer spectra of Fig. 3b, the relation I_{CN}/I_{Ar} has been calculated at different depths and the values are reported in Table 2. With the exception of up to 10 μm, the values of I_{CN}/I_{Ar} up to 60 μm of depth are very similar and show a good correlation with the value obtained for bulk *b*-St-co-MOP$_1$ copolymer, therefore these results confirm that the chemical composition of nanofibers is uniform through all the length of the nanocavity. This result is not trivial, since this methodology has revealed inhomogeneities along the nanopore, in other infiltrated systems [12]. The rather small difference in the values of I_{CN}/I_{Ar} for all the spectra can be caused by more local information of these measurements resulting from the depth resolution of the Raman instrument. Moreover, the discrepancy obtained in I_{CN}/I_{Ar} up to 10 μm maybe due to air interferences in confocal measurement, as recently being reported [39]. It has been reported that differences in the refractive index between air and the sample can cause

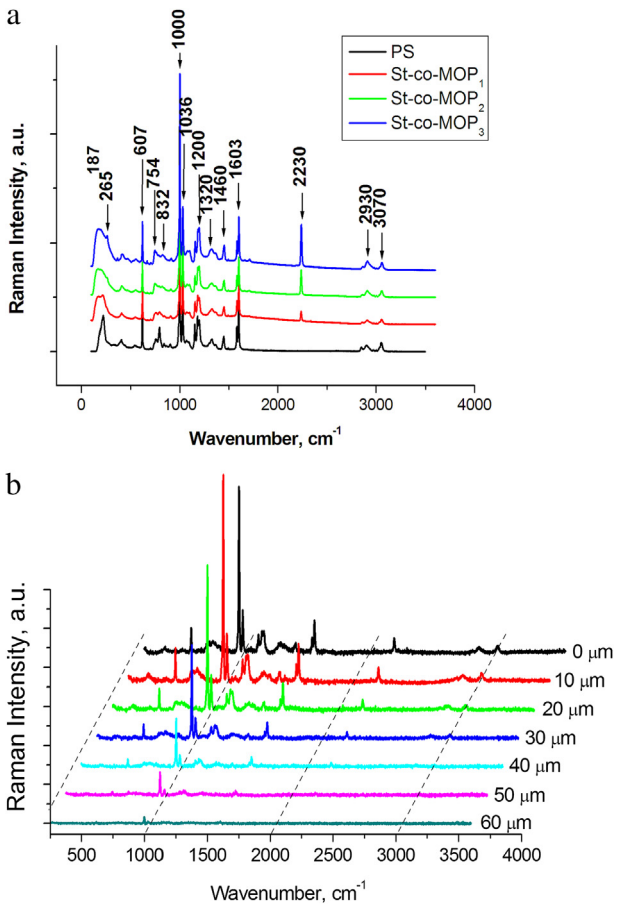

Fig. 3. (a). Raman spectra of *b*-St-co-MOP$_1$, *b*-St-co-MOP$_2$, *b*-St-co-MOP$_3$ and *b*-PS. (b) Raman spectra of *n*-St-co-MOP$_1$ with pinhole.

further errors in the obtained depth profile due to strong aberration effects. Be as maybe, Confocal Raman spectroscopy has allowed us to follow and identify the copolymer into AAO nanopores until 60 μm and to demonstrate that no changes in chemical composition by degradation or other chemical or physical process are observed.

3.5. Glass transition temperature

The segmental mobility of macromolecular chains is one of those polymer properties that could be of great importance in the use of nanofibers as scaffolds, for which very high or low T_g values would not be desirable. Differential scanning calorimetry study of copolymer nanofibers is shown in Fig. 4. The observed glass-transition region of copolymers in the AAO nanocavities is broader than that of bulk polymers, not shown here, this effect being similar for PS as described by other authors [40–42]. In

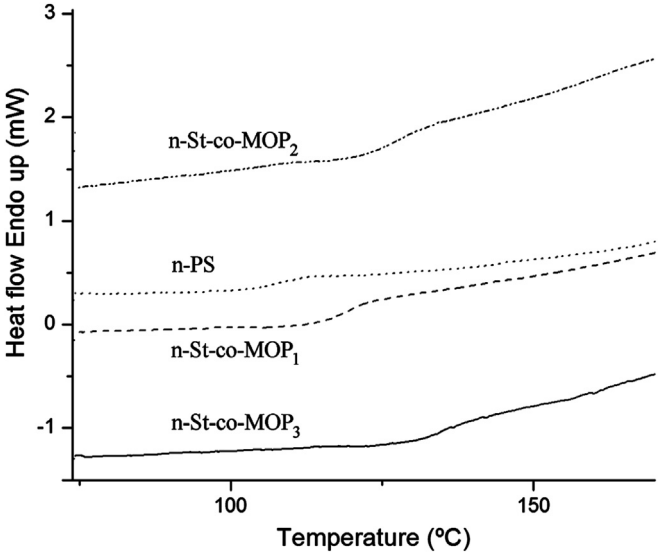

Fig. 4. DSC curves for *n*-St-co-MOP and *n*-PS.

Table 3 the glass transition temperature values of the nanostructured and bulk copolymers are collected. At a first glance, the T_g value for the nanostructured *n*-St-co-MOP and *n*-PS is higher than that of the corresponding bulk polymers, therefore, it is an indication of some dependence on confinement. Nevertheless, only scarce studies about the glass transition temperature of polymers confined AAO templates are reported in the literature, Shin et al., found confinement effects for polystyrene infiltrated in AAO templates and claimed that their results were similar to those of supported ultrathin films [41]. In general, most of the works in the literature suggest that confinement directly affects the cooperative movements of the polymer chains. Nevertheless, the results seem to be contradictory or at least not to follow a general rule. For instance, while for ultrathin films deviations from bulk T_g as large as 45–50 K (in supported films) and 70 K (in free-standing films) have been reported, Tress et al. found that, in the studies of glassy dynamics and glass transition in thin polymer layers of PMMA deposited on different substrates, the glassy dynamics was not altered due to the one-dimensional confinement in these thin polymer layers [39]. The same authors reported that, because some studies do not find thickness dependent shifts of the glassy dynamics, this implies that, in these cases, the preparative and experimental conditions were sufficient to avoid effects on the glassy dynamics of the polymer layers. Contrary to these works, Table 3 evidences that confinement increases the T_g values in all cases and, as a first approach, we can explain these results by the interaction of the copolymer with alumina of AAO templates. Moreover, further evidences that confinement effect increases the T_g values of polymers have been obtained by our group in the study

Table 2
Relations I_{CN}/I_{Ar} in confocal methodology for *n*-St-co-MOP1.

Profundity (μm)	I_{CN}/I_{Ar}
0	0.44 ± 0.03
10	0.36 ± 0.02
20	0.38 ± 0.03
30	0.40 ± 0.03
40	0.41 ± 0.03
50	0.42 ± 0.03
60	0.41 ± 0.03

Table 3
DSC studies for St-co-MOP and PS polymers.

Polymer	T_g half C_p extrapolated (°C)	Difference nano–bulk (°C)
b-PS	108 ± 1	2
n-PS	110 ± 1	
b-St-co-MOP$_1$	116 ± 1	2
n-St-co-MOP$_1$	118 ± 1	
b-St-co-MOP$_2$	123 ± 1	4
n-St-co-MOP$_2$	127 ± 1	
b-St-co-MOP$_3$	129 ± 1	4.5
n-St-co-MOP$_3$	133.5 ± 1	

of PMMA confined in AAO templates of different diameters. As has been reported by Steinhart et al., [3] changes in T_g are probably the most researched, with clear and intuitively expected indications of slowed-down segmental dynamics for the case of strongly absorbing surfaces but sometimes conflicting trends and a lack of understanding of the physical basis for the often decreased T_g close to free or nonabsorbing interfaces. In our results it is possible to see that the increment of F_{MOP} values increases the difference between T_g values for bulk and nanostructured copolymer. Probably because the cooperative mobility of the chain is reduced for the existence of intramolecular interactions due to presence of polar residues in the polymer chains as demonstrated by previous solution studies [31]. So, our results reinforce the idea of the necessity of systematic studies about the influence of confinement effect on the T_g of polymers in order to get quantitative understanding of chain mobility alterations due to geometric constraints.

3.6. Thermal stability

The examination through thermo gravimetric analysis has allowed us to study the thermal stability of nanofibers and to compare the properties of bulk and nanostructured copolymers. TG differential curves, expressed in % weight, for two selected copolymers, corresponding to the minimum and maximum value of F_{MOP}, *n*-St-co-MOP$_1$ and *n*-St-co-MOP$_3$ copolymers, under nitrogen and air atmosphere, are show in Fig. 5a and b, respectively. In a N_2 atmosphere, thermograms for all the samples only show one peak around 400 °C while the copolymers in an air atmosphere show two thermal events, the first peak being similar to that obtained in the N_2 atmosphere and a second onset peak at higher temperature, which is not present in the first case. Table 4 compares the values of *b*-St-co-MOP and *n*-St-co-MOP copolymers.

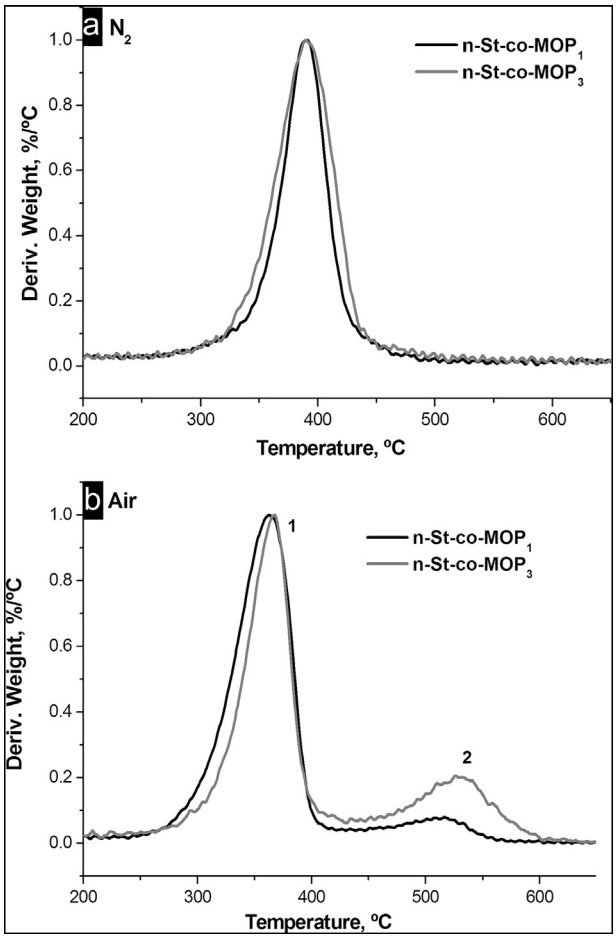

Fig. 5. TG differential curves, expressed in % weight, for *n*-St-co-MOP copolymers in nitrogen (a) and air (b) atmosphere.

As observed in Table 4, in nitrogen, the onset point values show differences between bulk and nanostructured copolymers. The temperature values of the peak are lower for nanostructured in comparison to bulk copolymers, so St-co-MOP copolymers confined in nanocavities are rather more unstable than in the bulk. This result could be explained by the alumina effect which would catalyze the decomposition of copolymers confined.

The existence of two thermal events in bulk copolymers when the decomposition is carry out in air is probably caused by the presence of tautomeric forms. As indicated by other authors, the presence of enol tautomers produces the stabilization in thermoxidative degradation. Mohamed has studied the effect of aromatic hydrazides as stabilizers for rigid PVC against thermo-oxidative degradation and found that the stabilization occurs in presence of enolic forms in the aromatic hydrazides [43]. These results are consistent with our previous studies conducted in different solvents, which demonstrated that our copolymers exhibit a higher content of enol form in more polar solvents, and favored the hydrogen bond interactions [31]. Thus, St-co-MOP copolymers in polar environments favor the displacement of tautomeric equilibrium towards the enolic form enable hydrogen bond interactions between enol form and alumina support (see Scheme S2 in Supporting Information). Table S1 presents the relation between percentage abundance of thermal events in the bulk and in the nanocopolymers. For nanostructured copolymers, the polar environment in AAO template displaces the equilibrium to enol form and for this reason the relation 2°/1° in nanostructured copolymer is higher than 2°/1° in bulk copolymer. So, this result indirectly evidences the effect of tautomeric equilibrium of the copolymers in nanocavities and opens the possibility to prepare attractive nanostructured surfaces based on tautomerizable copolymers which could discriminate against specific substrate.

3.7. Mechanical properties

The mechanical properties of nanofibers have been indirectly determined from the bulk copolymers, as no accessible equipment to characterize isolated nanofiber is available. Table 5 shows the mechanical properties evaluated for two copolymers in comparison to homopolymer (PS). It is possible to see that the inclusion of MOP inside a macromolecular structure significantly affect the resistance of the material as evaluated by the elastic moduli and ultimate tensile stress. The ultimate tensile stress increases with the increase of the MOP monomer mole fraction in the copolymer. The elastic moduli of the copolymers were in the range of cortical bone (17–20 GPa) and trabecular bone (50–100 MPa), while the tensile

Table 4
Thermo gravimetric analysis of St-co-MOP.

Atmosphere	Polymer		Onset point (1) (°C)	Second onset point (2) (°C)
N_2	Bulk	*b*-St-co-MOP$_1$	364 ± 1	–
		b-St-co-MOP$_3$	357 ± 1	–
	Nano	*n*-St-co-MOP$_1$	362 ± 1	–
		n-St-co-MOP$_3$	356 ± 1	–
Air	Bulk	*b*-St-co-MOP$_1$	334 ± 1	475 ± 1
		b-St-co-MOP$_3$	347 ± 1	523 ± 1
	Nano	*n*-St-co-MOP$_1$	325 ± 1	485 ± 1
		n-St-co-MOP$_3$	335 ± 1	491 ± 1

Table 5
Mechanical properties of analyzed polymers.

Polymer	Elongation-at-break (%)	Ultimate tensile stress (MPa)	Elastic modulus (MPa)
PS	7.7 ± 0.2	30 ± 1	1180 ± 30
St-co-MOP$_1$	21 ± 3	36 ± 3	2380 ± 90
St-co-MOP$_2$	8.9 ± 0.05	49 ± 6	1700 ± 200

Results are expressed as the mean ± SEM, $n = 3$.

strength reaches values intermediate between that of trabecular bone (5–10 MPa) and cortical bone (80–150 MPa) [44]. Roughly, the elastics modulus found for the bulk copolymers are consistent with their employment for building extracellular matrices.

4. Conclusions

By a simple infiltration process of the polymer in AAO templates, new keto-enol tautomerizable polystyrene copolymer nanofibers, i.e. styrene-co-2-methyl-3-oxo-5-phenyl-4-pentenonitrile (St-co-MOP) of different chemical composition, have been prepared. SEM characterization of St-co-MOP copolymer nanofibers, demonstrate a high degree of regularity along the entire length of nanofiber, as well as the association between extracted nanofibers caused by the stacking or possible interactions between them. We have characterized St-co-MOP tautomerizable copolymers by confocal Raman spectroscopy and analyzed the copolymer composition inside the nanopores until 60 μm of depth, showing the uniform filling of the nanocavities. Therefore, these results demonstrate that this is a suitable technique to study the chemical composition gradient of other copolymers or polymer blends in one dimension nanocavities. The effect of the nanoconfinement and of the tautomeric form of the copolymers on the thermal properties was put in evidence through the DSC and TGA studies, respectively. For all polymers, the values of T_g are higher for the nanostructured than for the corresponding bulk copolymers, suggesting the existence of interactions between infiltrated copolymers and alumina walls of AAO templates. By, thermo gravimetric analysis the presence of two thermal events in air has been detected, caused probably by the presence of tautomeric forms. Moreover, the elastics moduli found for the bulk copolymers are consistent with their employment for building extracellular matrices.

In summary, this work clearly demonstrates the feasibility of obtaining high production of styrene-co-2-methyl-3-oxo-5-phenyl-4-pentenonitrile (St-co-MOP) copolymers nanofibers and shows that the fact of the presence of keto-enol tautomerism in copolymers nanofibers can open the possibility to prepare attractive nanostructured surfaces which can discriminate against specific substrates. Currently, biocompatibility studies related with these materials are being carried out and do not show cytotoxic effects.

Acknowledgment

J.M. Giussi would like to thank La Plata National University and CONICET from Argentina and CSIC from Spain by the help granted for the collaboration. I. Blaszczyk-Lezak acknowledges support from CSIC for a JAE postdoctoral fellowship. Financial support from the MICINN, MAT2011-24797 and PRI-PIBAR-2011-1400 is also acknowledged.

The authors thank D. Gómez for SEM experiments and I. Muñoz for Raman measurements.

Appendix A. Supplementary data

Supplementary data related to this article can be found at http://dx.doi.org/10.1016/j.polymer.2013.06.040.

References

[1] Martín J, Maiz J, Sacristan J, Mijangos C. Polymer 2012;53:1149–66.
[2] Martín J, Mijangos C. Langmuir 2009;25:1181–7.
[3] Steinhart M, Wehrspohn RB, Gösele U, Wendorff JH. Angew Chem Int Ed 2004;43:1334–44.
[4] Chen D, Chen JT, Glogowski E, Emrick T, Russell TP. Macromol Rapid Commun 2009;30:377–83.
[5] Feng X, Jin Z. Macromolecules 2009;42:569–72.
[6] Mei S, Feng X, Jin Z. Macromolecules 2011;44:1615–20.
[7] Chen D, Zhao W, Wei D, Russell TP. Macromolecules 2011;44:8020–7.
[8] Palacios R, Formentín P, Ferré-Borrull J, Pallarés J, Marsal LF. Phys Status Solidi C 2009;6:1584–6.
[9] Ozaydin-Ince G, Gleason KK, Demirel MC. Soft Matter 2011;7:638–43.
[10] Martín J, Vázquez M, Hernández-Vélez M, Mijangos C. Nanotechnology 2008;19:175304.
[11] Martín J, Mijangos C, Sanz A, Ezquerra T, Nogales A. Macromolecules 2009;42:5395–401.
[12] Maiz J, Sacristan J, Mijangos C. Chem Phys Lett 2010;484:290–4.
[13] Lee DY, Lee DH, Lee SG, Cho K. Soft Matter 2012;8:4905–10.
[14] Duran H, Steinhart M, Butt HJ, Floudas G. Nano Lett 2011;11:1671–5.
[15] Michell RM, Lorenzo AT, Müller AJ, Lin M-C, Chen H-L, Blaszczyk-Lezak I, et al. Macromolecules 2012;45:1517–28.
[16] Martin J, Krutyeva M, Monkenbusch M, Arbe A, Allgaier J, Radulescu A, et al. Phys Rev Lett 2010;104:197801.
[17] Krutyeva M, Martin J, Arbe A, Colmenero J, Mijangos C, Schneider GJ, et al. J Chem Phys 2009;131:174901–11.
[18] Laslau C, Zujovic Z, Travas-Sejdic J. Prog Polym Sci 2010;35:1403–19.
[19] Richter S, Steinhart M, Hofmeister H, Zacharias M, Gösele U, Gaponik N, et al. Appl Phys Lett 2005;87:1–3.
[20] Pinto NT, Johnson Jr AT, MacDiarmid AG, Mueller CH, Theofylaktos N, Robinson DC, et al. Appl Phys Lett 2003;83:4244–6.
[21] Martín J, Vázquez M, Hernández-Vélez M, Mijangos CJ. Nanosci Nanotechnol 2009;9:5898–902.
[22] Dersch R, Steinhart M, Boudriot U, Greiner A, Wendorff JH. Polym Adv Technologies 2005;16:276–82.
[23] Jia H, Zhu G, Vugrinovich B, Kataphinan W, Reneker DH, Wang P. Biotechnol Prog 2002;18:1027–32.
[24] Kim BC, Nair S, Kim J, Kwak JH, Grate JW, Kim SH, et al. Nanotechnology 2005;16:S382–8.
[25] Grimm S, Martín J, Rodriguez G, Fernández-Gutierrez M, Mathwig K, Wehrspohn RB, et al. J Mater Chem 2010;20:3171–7.
[26] Cortizo AM, Ruderman G, Correa G, Mogilner IG, Tolosa EJ. J Biomater Tissue Engineer 2012;2:125–32.
[27] Wang B, Cai Q, Zhang S, Yang X, Deng X. J Mech Behav Biomed Mater 2011;4:600–9.
[28] Masuda S, Minagawa K. Prog Polym Sci 1996;21:557–91.
[29] Demetriu M, Krasia-Christoforou T. J Polym Sci Part A: Polym Chem 2012;50:52–60.
[30] Benner SA. Science 2004;306:625–6.
[31] Giussi JM, Allegretti PE, Cortizo MS. J Polym Sci A: Polym Chem 2012;50:4161–9.
[32] Masuda H, Yada K, Osaka A. Jpn J Appl Phys 1998;37:L1090–2.
[33] Hernandez-Velez H. Thin Solid Films 2005;495:51–63.
[34] Vázquez M, Pirota K, Hernández-Vélez M, Prida VM, Navas D, Sanz R, et al. J Appl Phys 2004;95:6642–4.
[35] Gauglitz G, Vo-Dinh T, editors. Handbook of spectroscopy. New York: Wiley-VCH; 2003.
[36] Blaszczyk-Lezak I, Maiz J, Sacristan J, Mijangos C. Ind Eng Chem Res 2011;50:10883–8.
[37] Du Y. Appl Phys Lett 1999;74:2951–3.
[38] Gallardo A, Spells S, Navarro R, Reinecke H. J Raman Spectrosc 2007;38:880–4.
[39] Tress M, Erber M, Mapesa EU, Huth H, Müller J, Serghei A, et al. Macromolecules 2010;43:9937–44.
[40] Roghani-Mamaqani H, Haddadi-Asl V, Najafi M, Salami-Kalajahi M. AIChE J 2011;57:1873–81.
[41] Shin K, Obukhov S, Chen JT, Huh J, Hwang J, Mok J, et al. Nat Mater 2007;6:961–5.
[42] Efremov MY, Olson EA, Zhang M, Zhang Z, Allen LH. Phys Rev Lett 2003;91:085703.
[43] Mohamed NA. Polym Degrad Stab 1997;56:317–29.
[44] Anseth KS, Shastri VR, Langer R. Nat Biotechnol 1999;17:156–9.